LETTERS

Hyperion's sponge-like appearance

P. C. Thomas[1], J. W. Armstrong[2], S. W. Asmar[2], J. A. Burns[1], T. Denk[3], B. Giese[4], P. Helfenstein[1], L. Iess[5], T. V. Johnson[2], A. McEwen[6], L. Nicolaisen[7], C. Porco[8], N. Rappaport[2], J. Richardson[1], L. Somenzi[5], P. Tortora[9], E. P. Turtle[10] & J. Veverka[1]

Hyperion is Saturn's largest known irregularly shaped satellite and the only moon observed to undergo chaotic rotation[1–3]. Previous work has identified Hyperion's surface as distinct from other small icy objects[4,5] but left the causes unsettled. Here we report high-resolution images that reveal a unique sponge-like appearance at scales of a few kilometres. Mapping shows a high surface density of relatively well-preserved craters two to ten kilometres across. We have also determined Hyperion's size and mass, and calculated the mean density as $544 \pm 50\,\mathrm{kg\,m^{-3}}$, which indicates a porosity of >40 per cent. The high porosity may enhance preservation of craters by minimizing the amount of ejecta produced or retained[6,7], and accordingly may be the crucial factor in crafting this unusual surface.

Hyperion orbits Saturn every 21.3 days with a semi-major axis of 24.55 Saturn radii. The Cassini spacecraft flew by Hyperion four times in 2005 and 2006 at ranges less than 300,000 km. A close fly-by in September 2005 was specifically targeted[8] to obtain high-resolution remote-sensing data and to track directly changes in the spacecraft trajectory caused by the mass of Hyperion.

Imaging during 2005 confirmed the expectations[1–3,9,10] of chaotic rotation, and showed that the object remains in an average spin state similar to that observed by Voyager: rotating nearly about the long axis, at ~72°–75° per day (see Supplementary Information). Cassini observations demonstrate that the spin vector moves through the body and across the sky; the subsolar latitude varied by 70° over the year of observations. The movement of the spin vector through the body meant that a global shape model (Fig. 1) could be constructed only by merging several partial models determined for each of the different encounters. The resulting model has a mean radius of 135 ± 4 km, with radii from the centre of figure between 95 and 182 km (Table 1). The uncertainty in the mean radius, hence of the volume, derives largely from errors in combining the partial shape models.

Hyperion's mass was obtained from measurements of the spacecraft velocity during the close encounter on 25 September 2006. Measurements entailed the transmission from the ground of a highly stable, almost monochromatic signal at 7.2 GHz and its coherent retransmission to Earth at 8.4 GHz and 32.5 GHz. Significant measurement noise, about 8–10 times larger than in previous Cassini radio science experiments[11] was due to the small solar elongation angle (55°) and the lack of a Ka-band uplink carrier.

The spacecraft fly-by took place at a closest approach distance of 618 km, and a relative velocity of $5.6\,\mathrm{km\,s^{-1}}$. The resultant change in the spacecraft velocity was about $0.1\,\mathrm{m\,s^{-1}}$, much larger than the measurement noise. The observed Doppler data were fitted with a dynamical model that included the gravitational acceleration from all Saturn system bodies and the non-gravitational accelerations. Thirteen parameters were fitted, namely the components of Cassini and Hyperion state vectors at a reference epoch, and the satellite's GM value, where G is the gravitational constant and M the mass.

A stable orbital solution was obtained resulting in a GM of $0.375 \pm 0.003\,\mathrm{km^3\,s^{-2}}$. The corresponding mass M, assuming $G = 6.6742 \times 10^{-11}\,\mathrm{m^3\,kg^{-1}\,s^{-2}}$, is therefore $5.619 \pm 0.050 \times 10^{18}$ kg. This value is in agreement with an independent estimate derived by the Cassini navigation team using a different method of orbit determination[8].

Hyperion has a mean density of $544 \pm 50\,\mathrm{kg\,m^{-3}}$; the uncertainty derives largely from the volume measurement. The mean density indicates a porosity of $42 \pm 6\%$ if Hyperion is primarily water ice[12]. Any significant contributions from higher density components increase the porosity. Hyperion's density is similar to that obtained for smaller satellites orbiting near the rings ($360–690\,\mathrm{kg\,m^{-3}}$; 15–89 km mean radii[13]), but only one-third that of Phoebe[14] ($1{,}630\,\mathrm{kg\,m^{-3}}$), the one other small object imaged by Cassini at similar resolutions and phase angles.

The most striking visual aspect of Hyperion is its sponge-like appearance (Fig. 1a, h) which is unlike that of any other object imaged to date and was not suggested[4,5] in the low-resolution Voyager images, although Hyperion had an intermediate albedo, spotted colour distribution, and topography that differed from those of other small icy satellites[4,5]. We measured the sizes of impact features: depressions that have distinct rim morphology, cut other forms and are approximately circular. After tabulating the obvious craters, few depressions remained, and we conclude that the sponge-like appearance is primarily manifested in the density of well-preserved craters 2–10 km in diameter. The area density of Hyperion craters exceeding 10 km in size, near 'empirical saturation'[15], is similar to that on Phoebe (Fig. 2a). On both objects the crater density decreases for craters between 10 km and 1 km in diameter, which is probably a reflection of a production function[14] with 'cookie cutter' removal of small craters by larger ones. For craters with diameters between 2 km and 11 km, Hyperion has a cumulative number of craters per unit area twice that on Phoebe; at similar resolution these objects are strikingly different (Fig. 1g, h).

Enhanced preservation of craters in this size range on Hyperion is probably the key to Hyperion's appearance. Craters may be eroded or otherwise rendered uncountable either through covering by ejecta, direct erasure by other craters, erosion by very small craters, or other effects such as sublimation. Hyperion displays little evidence of ejecta, and there is positive evidence that the retained ejecta volume

[1]Center for Radiophysics and Space Research, Cornell University, Ithaca, New York 14853, USA. [2]Jet Propulsion Laboratory, California Institute of Technology, Pasadena, California 91109, USA. [3]Institut für Geologische Wissenschaften, Freie Universität, 12249 Berlin, Germany. [4]Institute of Planetary Research, German Aerospace Center, Rutherfordstrasse 2, 12489 Berlin, Germany. [5]Dipartimento di Ingegneria Aerospaziale ed Astronautica, Università La Sapienza, via Eudossiana 18, 00184 Roma, Italy. [6]Department of Planetary Sciences, University of Arizona, Tucson, Arizona 85721, USA. [7]Physics and Astronomy Department, University of California at Los Angeles, Box 951547 Los Angeles, California 90095, USA. [8]Space Science Institute, 4750 Walnut Street, Boulder, Colorado 80301, USA. [9]DIEM-II Facoltà di Ingegneria, Università di Bologna, Via Fontanelle, 4047100 Forlì, Italy. [10]Johns Hopkins University Applied Physics Laboratory, 11100 Johns Hopkins Road, Laurel, Maryland 20723, USA.

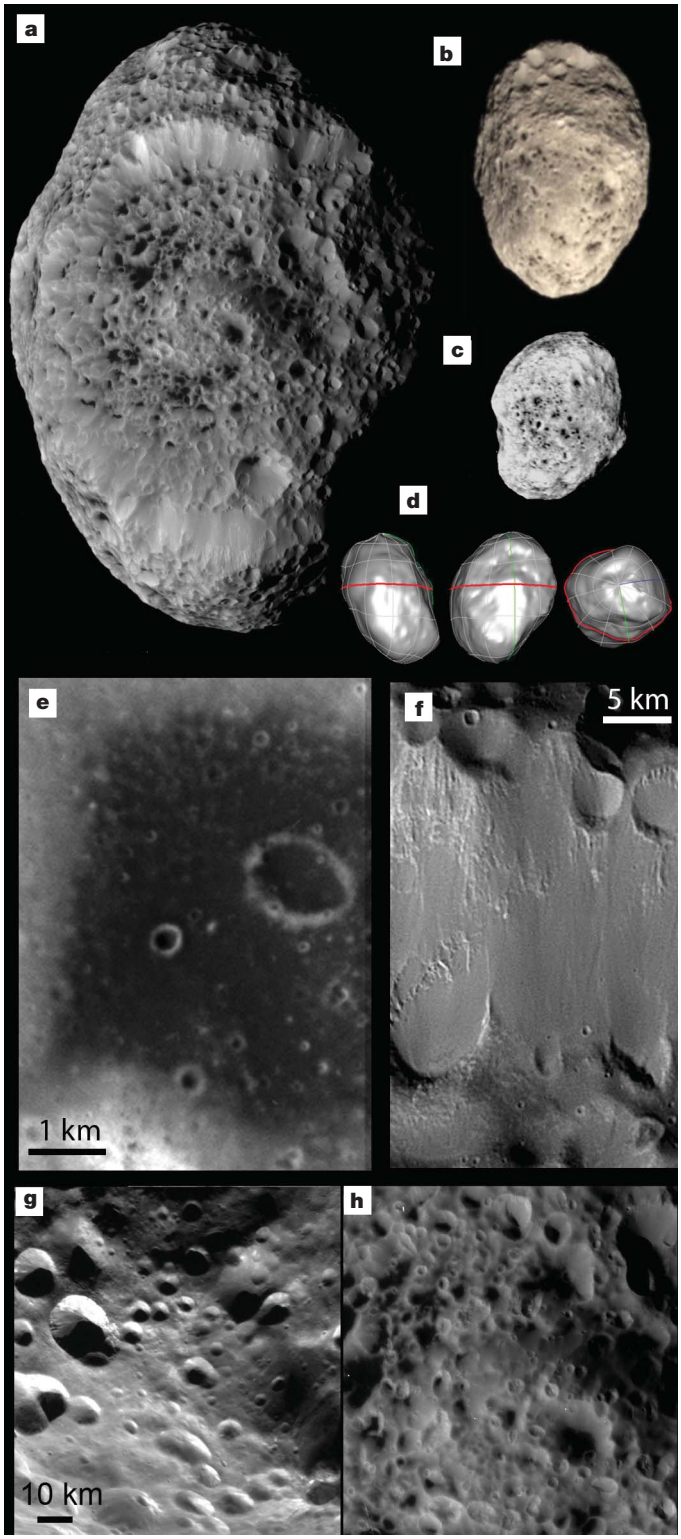

Figure 1 | Surface features of Hyperion. **a**, Full disk view, 300 km top to bottom, showing the sponge-like appearance and distribution of darker material in craters. The image includes the largest probable impact feature. Image N15506383386, range = 62145 km, solar phase angle $\alpha = 51.5^\circ$. **b**, Colour composite showing side opposite to that shown in **a** from images N1530199676, N1530199776 and N1530199809. **c**, Image N1497114664, showing partial profile of 120-km crater (left side). From 212000 km, $\alpha = 12.9^\circ$. **d**, Orthogonal views of the shape model of Hyperion. The latitude–longitude grid is relative to the early Revolution 15 spin vector, UTC 2005, 268/04:29:06 to 268/17:20:16 (see Supplementary Information). **e**, Dark floor of old crater, showing large number of sub-kilometre craters. Contrast has been greatly enhanced by both high-pass filtering and stretching; brighter rims are dark compared to average Hyperion. Portion of image N1506393614. **f**, Slopes of the 240-km diameter crater, showing smaller crater (left side) elongated upslope, partial burial of other craters, and rugged upper rim. Portion of image N1506391600. **g**, Phoebe, image N1465669953, 0.195 km per pixel, $\alpha = 83.7^\circ$. **h**, Hyperion, image N1506388580, 0.197 km per pixel, $\alpha = 51.1^\circ$.

Table 1 | Properties of Hyperion

Property	Value
Mean radius	135 ± 4 km
Range of radii	95–182 km
Mass	$(5.619 \pm 0.050) \times 10^{18}$ kg
Mean density	544 ± 50 kg m^{-3}
Range of gravitational heights	0–43.8 km
Range of surface acceleration	1.7–2.1 cm s^{-2}

Gravitational heights are heights above an equipotential surface.

is small. Old crater floors are themselves heavily cratered (Fig. 1e), as shown by slightly brighter rims visible with strong contrast enhancement. The survival of these short rims (likely to have been less than 15 m in height[16,17]) shows that the large craters have experienced less than ~20 m of deposition or erosion. The distinct visibility of narrow rim zones on craters, even ones cut by younger impacts, suggests the presence of structural rims unaffected by superposed ejecta. Ejecta blocks are scarce compared to Phoebe[14].

High porosity may contribute to the apparent minimal effects of ejecta either by suppressing production and dispersal outside the crater[6] or by enhanced velocity of material, such that most escapes the body[7]. Experiments and scaling theory predict that impacts into high-porosity targets produce less ejecta mass if the craters are primarily produced by compression rather than excavation[6]. A crucial part of these predictions is the role of gravity, parameterized by gD, where g is the local acceleration due to gravity, and D is the crater diameter. For a target of given porosity, the larger gD is, the smaller is the ratio of ejecta to crater volume. For a particular gD, at higher porosities the ejecta ratio is predicted to decrease partly by increased compression and partly by lower ejection velocities that allow more material to fall within the crater. Porosities below 30% have little effect on ejecta production, those over 40% can reduce ejecta by factors of more than four. Assuming the modelling results[6], Fig. 2b predicts that among observed targets Hyperion should have the most significant porosity effects on ejecta volumes. A different role for porosity has been suggested[7] wherein enhanced ejecta velocities cause escape from the target body. The only empirical information on cratering on a highly porous object comes from the Deep Impact experiment[18] on an object of radius 3 km with a porosity of probably >50%. Although it is unclear how large a fraction exceeded the escape velocity of ~1.3 m s^{-1}, it is likely that at least a modest fraction was retained[18,19]. Hyperion's escape velocity ranges from 45 m s^{-1} to 99 m s^{-1} depending upon location, and thus it may be difficult for large fractions of any ejecta produced to escape.

It is unlikely that unusual crater depths significantly enhance the sponge-like appearance. Crater depth-to-diameter ratios for the 13 examples that can be measured reliably using shadow lengths average 0.21 ± 0.05 (s.d.). These ratios are similar to values for fresh lunar craters[16], and are slightly greater than for some small rocky objects[20]. They are slightly larger than that for craters on large icy satellites, 0.14 (ref. 21).

Adding to the unusual appearance of Hyperion are dark surfaces in the floors of degraded craters (Fig. 1). These have broadband-visible (0.56 μm) albedos a factor of ~4 less than the average value of ~0.5 for Hyperion. The dark materials are slightly redder than brighter areas: UV/GRN (0.338 μm/0.568 μm) = 0.61 for dark areas and 0.65 for bright slopes. IR3/GRN (0.930 μm/0.568 μm) ratios are ~1.3 for bright areas; 1.6 for dark ones. These colours suggest mixing of brighter and darker materials broadly similar to that seen on some other dark Saturnian satellites[22]. Dark floors are largely absent from fresher craters and avoid regional slopes of >15°. Margins of the low-albedo areas are gradational; there are no exposed dark layers, no

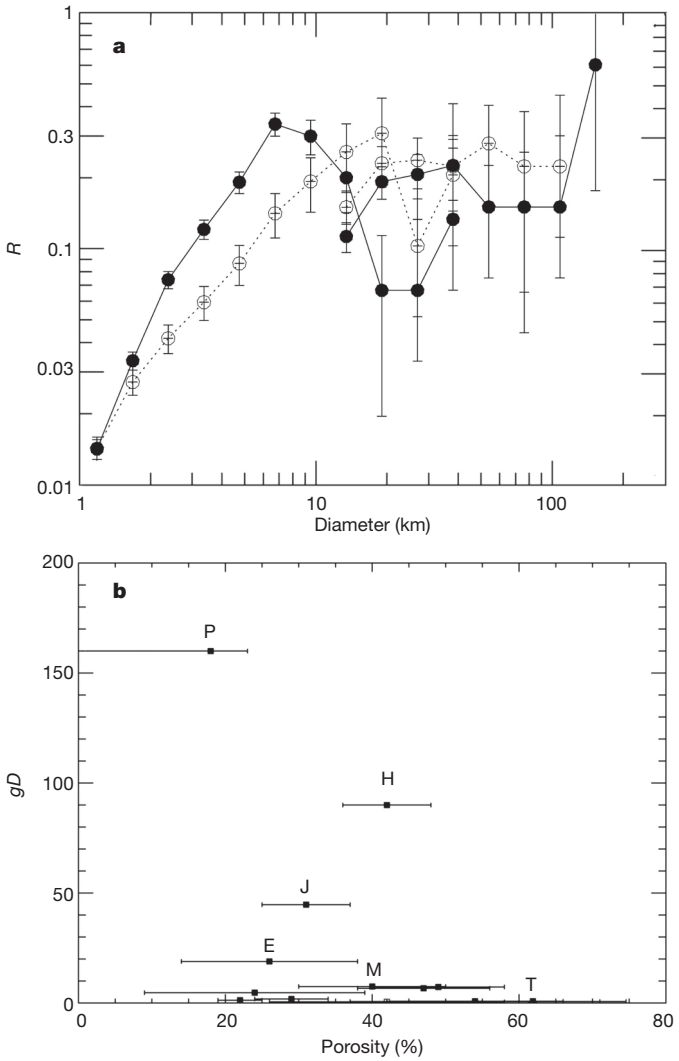

Figure 2 | Impact crater characteristics and conditions on Hyperion. a, Area density of craters on Hyperion and Phoebe. Solid symbols are Hyperion data; open symbols are for Phoebe. Data are restricted to diameters >1 km; resolution of data extending to 1 km is approximately 100 m per pixel. Error bars are from $\sqrt{n}$ scaling, where n is the number of craters in each size bin. $R = [(D_a D_b)3/2]^*[N_a/(D_b - D_a)]$ where D_a and D_b are crater diameter ranges, $D_b > D_a$ and N_a is the number of craters per unit area. **b**, Porosity and gravity parameter for well-imaged objects. gD is local gravity times crater diameter of one-third the object mean radius (cm s^{-2} km). Porosity below 30% is predicted to have little effect on ejecta volume[6]. Comparison objects are labelled with the first letters of Phoebe, Janus, Epimetheus, Mathilde, and Tempel-1; others include Phobos, Deimos, Ida, Pan, Atlas, Prometheus and Pandora. Porosities and gD calculated from information in refs 13, 14, 28–30. gD for Hyperion is 3,000 times that for Tempel-1. Error bars reflect uncertainties in mean density apart from uncertainties in composition. For Phoebe, the lower bound of 0% reflects uncertainty in composition.

morphologically distinct mounds of dark material, and no collections of dark material at the base of the large slopes in the largest crater (Fig. 1f). The distribution and gradational margins of the dark material are consistent with downslope motion of surficial materials. Macroscopic compositional layering or other segregation of different components in the 'bedrock' is not seen on Hyperion. There are no bright-rayed craters, nor are there exposures of distinct brighter or darker layers in Hyperion's crater walls as on Phoebe[14]. Downslope movement of material other than that in the dark-floored depressions is shown by a few crater-wall streamers, crater-filling on long slopes, and some slumping inside craters. The lack of any clear segregation of different materials suggests that if the dark material is intrinsic to Hyperion it is mixed nearly uniformly at a small scale. Any exogenous dark material, such as debris from Phoebe or other outer satellites[23] would be evenly distributed initially and subsequently concentrated even by small amounts of downslope transport.

Could sublimation, enhanced by the dark material, contribute to deepening and widening the craters[24] to give Hyperion's distinctive appearance? Our measurements show that craters 2–10 km in diameter have depths of >400 m. Deepening by sublimation would have to be over 100 m, and widening would have to be several hundreds of metres to make a visible morphological difference. Approximate scaling from modelling of Ceres[25], Callisto[26] and comets[27] suggests that at Saturn's distance from the Sun, dark water ice will sublimate much less than 10 m over the period of existence of the Solar System so far, even allowing for some concentration of incident radiation at the bottom of depressions. CO_2 is far more volatile[26,27], and has been detected on Hyperion[24]. However, the restriction of erosional effects to <20 m may limit the amount of CO_2 available to sublimate. Thus, although sublimation and downslope motion may affect the distribution of dark material, primary crater morphology rather than sublimation dictates the unusual appearance of Hyperion.

Received 15 January; accepted 23 March 2007.

1. Klavetter, J. J. Rotation of Hyperion. I—Observations. *Astron. J.* **97,** 570–579 (1989a).
2. Klavetter, J. J. Rotation of Hyperion. II—Dynamics. *Astron. J.* **98,** 1855–1874 (1989b).
3. Black, G. J., Nicholson, P. D. & Thomas, P. C. Hyperion: rotational dynamics. *Icarus* **117,** 149–161 (1995).
4. Smith, B. A. *et al.* A new look at the Saturn system: the Voyager 2 images. *Science* **215,** 504–537 (1982).
5. Thomas, P. C., Black, G. J. & Nicholson, P. D. Hyperion: Rotation, shape, and geology from Voyager images. *Icarus* **117,** 128–148 (1995).
6. Housen, K. R. & Holsapple, K. A. Impact cratering on porous asteroids. *Icarus* **163,** 102–119 (2003).
7. Asphaug, E., Ryan, E. V. & Zuber, M. T. in *Asteroids III* (eds Bottke, W. F., Cellino, A., Paolicchi, P. & Binzel, R. P.) 463–484 (Tucson, Univ. Arizona Press, 2002).
8. Criddle, K. E. *et al.* Cassini orbit determination: the only targeted Hyperion flyby of the prime mission. *29th Annual AAS Guidance and Control Conference (Breckenridge, Colorado)* AAS Paper~06–082 (American Astronomical Soceiety, San Diego, California, 2006).
9. Wisdom, J., Peale, S. J. & Mignard, F. The chaotic rotation of Hyperion. *Icarus* **58,** 137–152 (1984).
10. Binzel, R. P., Green, J. R. & Opal, C. B. Chaotic rotation of Hyperion? *Nature* **320,** 511 (1986).
11. Armstrong, J. W., Iess, L., Tortora, P. & Bertotti, B. Stochastic gravitational wave background: upper limits in the 10^{-6}-10^{-3} Hz band. *Astrophys. J.* **599,** 806–813 (2003).
12. Clark, R. N., Fanale, F. P. & Gaffey, M. J. in *Satellites* (eds Burns, J. A. & Mathews, M. S.) 437–491 (Tucson, Univ. Arizona Press, 1986).
13. Porco, C. C. *et al.* Physical characteristics and possible accretionary origins for Saturn's small satellites. *Annu. Lunar Planet. Sci. Conf.* **37,** 2289 (2006).
14. Porco, C. C. *et al.* Cassini imaging science: initial results on Phoebe and Iapetus. *Science* **307,** 1237–1242 (2005).
15. Chapman, C. R. *et al.* Impact history of Eros: craters and boulders. *Icarus* **155,** 104–118 (2002).
16. Pike, R. J. in *Impact and Explosion Cratering* (eds Roddy, D. J., Pepin, R. O. & Merrill, R. B.) 484–509 (Pergamon, New York, 1977).
17. Melosh, H. J. *Impact Cratering: A Geologic Process* 1–253 (Oxford Monographs on Geology and Geophysics, No. 11, Oxford Univ. Press, New York, 1989).
18. Richardson, J. E. & Melosh, H. J. Determining comet Tempel 1's gravity, mass, and density via the ballistic behavior of the Deep Impact ejecta plume. *Icarus* (submitted).
19. Sugita, S. *et al.* Subaru telescope observations of Deep Impact. *Science* **310,** 274–278 (2005).
20. Carr, M. H. *et al.* The geology of Gaspra. *Icarus* **107,** 61–71 (1994).
21. Schenk, P. M. Ganymede and Callisto—Complex crater formation and planetary crusts. *J. Geophys. Res.* **96,** 15635–15664 (1991).
22. Buratti, B. J., Hicks, M. D. & Davies, A. Spectrophotometry of the small satellites of Saturn and their relationship to Iapetus, Phoebe, and Hyperion. *Icarus* **175,** 490–495 (2005).
23. Cruikshank, D. P. *et al.* The dark side of Iapetus. *Icarus* **53,** 90–104 (1983).
24. Cruikshank, D. P. *et al.* Surface composition of Hyperion. *Nature* doi:10.1038/nature05948 (this issue).
25. Fanale, F. P. & Salvail, J. R. The water regime of asteroid (1) Ceres. *Icarus* **82,** 97–110 (1989).
26. Moore, J. M. *et al.* Mass movement and landform degradation on the icy Galilean satellites: results of the Galileo nominal mission. *Icarus* **240,** 294–312 (1999).

27. Delsemme, A. H. in *Comets* (ed. Wilkening, L. L.) 85–130 (Tucson, Univ. Arizona Press, 1982).
28. Richardson, J. E., Melosh, H. J., Greenberg, R. J. & O'Brien, D. P. The global effects of impact-induced seismic activity on fractured asteroid surface morphology. *Icarus* **179,** 325–349 (2005).
29. Thomas, P. C. *et al.* Mathilde: size, shape, and geology. *Icarus* **140,** 17–27 (1999).
30. Thomas, P. C. Gravity, tides, and topography on small satellites and asteroids—Application to surface features of the Martian satellites. *Icarus* **105,** 326–244 (1993).

Supplementary Information is linked to the online version of the paper at www.nature.com/nature.

Acknowledgements Technical assistance was provided by B. Carcich, K. Consroe, P. Smith and P. F. Helfenstein. G. Patton checked the crater tabulation on Phoebe and Hyperion. This work was funded in part by the Cassini project. A portion of this work was done at the Jet Propulsion Laboratory, California Institute of Technology, under a contract from NASA. The work of L.I., P.T. and L.S. was funded in part by the Italian Space Agency. The manuscript benefited from reviews by K. Housen and E. Asphaug.

Author Information Reprints and permissions information is available at www.nature.com/reprints. The authors declare no competing financial interests. Correspondence and requests for materials should be addressed to P.C.T. (pct2@cornell.edu).

Supplementary Table S1 : Instantaneous spin solutions:

UTC range	RA	Dec	Rate	SS lat
2005,160/18:10:05 - 161/09:58:38	208.4	35.3	75	-14.1
2005,161/16:43:20 - 162/15:22:01	210.8	39.3	75	-13.3
2005,228/01:46:59 - 228/20:16:46	271.3	35.6	72	27.0
2005,228/22:16:13 - 229/12:15:23	266.7	39.1	72	22.1
2005,268/04:29:06 - 268/17:20:16	315.1	56.6	72	13.3
2005,268/17:20:16 - 269/02:18:20	299.8	58.7	72	11.3
2006,179/02:24:03 - 180/04:15:09	184.5	34.8	72	-43.7

UTC: year, day, hour, minute, second
Rotation rate is in degrees per day.
SS lat: Sub solar latitude, in degrees.
Spin solutions obtained by location of control points, mostly crater rims, and interactively solving for spin orientation, and body-centered coordinates of the control points. Uncertainties in these instantaneous vectors are approximately 2 degrees.